NANO · MICRO small
www.small-journal.com

Cell-Derived Vesicles for Antibiotic Delivery—Understanding the Challenges of a Biogenic Carrier System

*Eilien Heinrich, Olga Hartwig, Christine Walt, Arefeh Kardani, Marcus Koch, Leila Pourtalebi Jahromi, Jessica Hoppstädter, Alexandra K. Kiemer, Brigitta Loretz, Claus-Michael Lehr, and Gregor Fuhrmann**

Recently, extracellular vesicles (EVs) sparked substantial therapeutic interest, particularly due to their ability to mediate targeted transport between tissues and cells. Yet, EVs' technological translation as therapeutics strongly depends on better biocompatibility assessments in more complex models and elementary in vitro–in vivo correlation, and comparison of mammalian versus bacterial vesicles. With this in mind, two new types of EVs derived from human B-lymphoid cells with low immunogenicity and from non-pathogenic myxobacteria SBSr073 are introduced here. A large-scale isolation protocol to reduce plastic waste and cultivation space toward sustainable EV research is established. The biocompatibility of mammalian and bacterial EVs is comprehensively evaluated using cytokine release and endotoxin assays in vitro, and an in vivo zebrafish larvae model is applied. A complex three-dimensional human cell culture model is used to understand the spatial distribution of vesicles in epithelial and immune cells and again used zebrafish larvae to study the biodistribution in vivo. Finally, vesicles are successfully loaded with the fluoroquinolone ciprofloxacin (CPX) and showed lower toxicity in zebrafish larvae than free CPX. The loaded vesicles are then tested effectively on enteropathogenic *Shigella*, whose infections are currently showing increasing resistance against available antibiotics.

1. Introduction

Extracellular vesicles (EVs) are nanosized structures, which originate from various cell types, and can be found in different tissues and fluids of the human body. There are different types of EVs depending on their origin within the cell, for instance exosomes which are formed in endosomal compartments and microvesicles formed by budding of the cell membrane.[1] While ascertaining the exact biogenesis of these vesicles is extraordinarily difficult, the umbrella term of EVs is established within the research community and will be continued to be used here when mammalian vesicles are addressed.[2] Gram-negative bacteria are also generating a type of vesicle, called outer membrane vesicles (OMVs) whose structural elements and content are comparable to that of their bacterial origin.[3,4] Roughly summarizing, both types of vesicles consist of a phospholipid bilayer and contain, depending on their origin, nucleic acids, proteins, and enzymes. The main biological function of mammalian or bacterial vesicles is to deliver content, enabling the cargo to be transported for longer distances, protected from the environment.[5] This allows EVs to be involved in tissue repair or immune modulation by transporting miRNA or antigens for example.[6,7] In pathogens, OMVs play a crucial role in the transfer of resistances, transport of degrading enzymes, or genetic information.[8,9] OMVs may also influence biofilm formation and architecture, providing an alternative treatment avenue for such difficult-to-treat infections.[10] With this in mind, it was only a matter of time that EVs and OMVs were considered as potential therapeutics, such as drug delivery systems.

E. Heinrich, O. Hartwig, C. Walt, A. Kardani, B. Loretz, C.-M. Lehr, G. Fuhrmann
Helmholtz-Institute for Pharmaceutical Research Saarland (HIPS)
Helmholtz-Centre for Infection Research (HZI)
Campus E8.1, 66123 Saarbrücken, Germany
E-mail: gregor.fuhrmann@fau.de

The ORCID identification number(s) for the author(s) of this article can be found under https://doi.org/10.1002/smll.202207479.

DOI: 10.1002/smll.202207479

E. Heinrich, O. Hartwig, C. Walt, A. Kardani, J. Hoppstädter, A. K. Kiemer, C.-M. Lehr, G. Fuhrmann
Department of Pharmacy
Saarland University
Campus E8.1, 66123 Saarbrücken, Germany

M. Koch
INM – Leibniz Institute for New Materials
Campus D2 2, 66123 Saarbrücken, Germany

L. P. Jahromi, G. Fuhrmann
Friedrich-Alexander-University Erlangen-Nürnberg
Department of Biology
Pharmaceutical Biology
Staudtstr. 5, 91058 Erlangen, Germany

In the field of infectious diseases, nanocarriers as drug delivery systems have been shown to address problems such as solubility, bioavailability and targeted antibiotic therapy.[11] Especially the release of high drug doses by fusion with bacterial membranes,[12] and specifically targeting pathogens through surface interactions to combat resistance mechanisms, are two of many advantages of nanocarrier.[13] Indeed, before the commercialization of the first antibiotic penicillin, infectious diseases were the leading cause of death, in particular pneumonia, tuberculosis and gastrointestinal infections.[14] In recent years, the number of newly approved antibiotics constantly declined and pathogens continued to progressively develop resistances, such as the methicillin resistant *Staphylococcus* or the vancomycin resistant *Enterococcus*.[15] *Shigella* infections, for instance cause 164 000 deaths annually with a severe clinical picture of bloody mucoid stool, finalizing in a sepsis.[16] The inadequate use of antibiotics accompanied by the mode of action of *Shigella flexneri*, where they infest intestinal epithelial and immune cells and escape the antibiotic treatment, results in increasing resistance to commonly used therapeutics.[17] The resistance rates to the first line fluoroquinolone ciprofloxacin (CPX) have increased up to 1% in Europe, 29% in Asia–Africa[18] and 44% specifically in Bangladesh.[19,20] As a result, the World Health Organization has listed antimicrobial resistance as one of the severe threats to our society.[21,22] Since the development of new antibiotics is stagnating, there is an urgent need to explore new treatment concepts, such as nanocarrier drug delivery systems. However, these synthetic nanocarriers also bear the potential to induce immunogenicity and depleted efficacy during long-term therapy.[13] Although the safety of commonly used materials has already been proven, the introduction of new, more advanced synthetic compositions poses additional challenges in terms of biocompatibility and toxicity.[23] Such considerations have also triggered the search for biogenic alternatives, such as cell-derived EVs.[24]

Although in the past decades many reports on characterization and drug delivery applications of EVs and OMVs have been published,[25,26] it becomes clear that industrial and clinical translation is only feasible when different challenges are addressed. These include i) more comparative studies between mammalian and bacterial vesicles as carrier platforms, ii) advanced biocompatibility assessments using complex 3D cell culture and animal models, and iii) in vitro–in vivo correlation to optimize carrier properties. In this work, we will shine light on some of these aspects by providing fundamental comparison of different EVs in various in vitro and in vivo settings. Vesicles were loaded with model antibiotic CPX, as this had not been reported previously. The clinical use of CPX is currently the subject of an intense debate because of increasing bacterial resistances toward fluoroquinolones and occurrence of side effects, especially in the case of *Shigella* infections.[27] We specifically chose to assess such a challenging drug in in vitro and in vivo settings and studied how loading into EVs influences the drugs biocompatibility.

In our study, we present a head-to-head comparison of OMVs derived from the myxobacterial strain SBSr073 (SB-OMVs) and EVs derived from B-lymphoid RO cells (RO-EVs). We identified challenges in the loading of model drug CPX using various encapsulation techniques. The biocompatibility of vesicles was evaluated on human primary immune cells and in a *Danio rerio* embryo model to draw a complex overall picture. The drug-loaded vesicles were able to inhibit the growth of *S. flexneri* pathogens in vitro. We then investigated the biodistribution pattern of vesicles in an advanced three-dimensional cell culture model composed of epithelial and immune cells. Concluding in vivo evaluations in zebrafish larvae were able to verify an amplified accumulation of vesicles in immune cells. Overall, our study is a building block for a better understanding of EVs and underlines that their clinical translation is complex, in particular for antibiotic avenues.

2. Results and Discussion

2.1. Isolation and Characterization of Vesicles

Two different types of EVs derived from the myxobacterial strain SBSr073 and B-lymphoid RO cells were purified from cell culture supernatant by differential ultracentrifugation with size exclusion chromatography (SEC), an established method in the field of EV research.[2] RO cells have a potentially favorable biocompatibility because they are isolated from a severe combined immunodeficiency patient and lack MHC class II molecules.[28] SBSr073 are non-pathogenic myxobacteria, which produce recently characterized OMVs[4,29] and can be scaled up easily. RO cells were cultured in serum free medium for several passages, without alterations in their morphology or cell viability (Figure S1, Supporting Information). EVs were isolated fortnightly, which reduces medium exchange to a minimum or time-consuming depletion of interfering vesicles from serum supplements. Cells were cultured in an upright position with volumes up to 70 mL, reducing plastic waste—compared to common culture conditions of, e.g., hMSC—by half, and storage capacity compared to common culturing techniques.[29] SBSr073 myxobacteria were cultured in glass flasks up to 500 mL and non-expensive media were used, paving the way for sustainable upscale production of vesicles. For both EV types, the most concentrated SEC fraction with $\approx 10^{12}$ mL^{-1}, determined by nanoparticle tracking analysis was then used for further experiments.

SB-OMVs and RO-EVs have been characterized regarding their physico-chemical characteristics (Figure S2, Supporting Information). The average size of vesicles was 194 nm for SB and 160 nm for RO, which is in agreement with values reported in literature.[24] SB-OMVs had a lower protein content than the RO-EVs (3.6 µg per particle, compared to 6.5 µg per particle), which is possibly related to the difference in zeta potential (−6.8 mV and −12.8 mV, respectively) RO-EVs were additionally characterized for surface markers CD9 and CD63 (Figure S2d,e, Supporting Information), according to MISEV regulations.[2] For SB-OMVs, no common protein markers are yet established, as the SBSr037 strain has only recently been identified.

2.2. Biocompatibility Considerations In Vitro and In Vivo

EVs are broadly claimed to have a low immunogenicity because of their cellular origin. And although several examples confirm

this—such as EVs secreted by cardiac-derived adherent proliferating cells as a new therapeutic in cardiac regeneration[30]—a generalization should be avoided. OMVs, which are shed from Gram-negative bacterial cells, have frequently been shown to be immunogenic. For instance, OMVs derived from pathogenic bacteria such as *Porphyromonas gingivalis* induced chronic periodontitis, and activated inflammasome complexes with high interleukin (IL)-1 beta secretion.[31] Thus, we were subsequently interested to better understand the vesicles' immunogenic potential and first performed an endotoxin gel clot assay. This method is generally recommended by the Food Drug Administration and the European Medicines Agency, and anchored in several pharmacopoeia for evaluating the quality and safety of pharmaceutical products.[32] Endotoxins, also known as lipopolysaccharides (LPS), are particularly associated with Gram-negative bacteria and their outer membrane. These O-antigen, oligosaccharide and lipid A structures activate Toll-like-receptor 4 on immune cells and induce production of pro-inflammatory cytokines. For injectables, regulatory agencies allow an endotoxin concentration below 0.25 EU mL^{-1} or 5 EU kg^{-1}.[33] In our gel clot assay both aseptically prepared vesicle pellets did not induce a firm gel formation, even at the highest concentration (Figure S3, Supporting Information). Although, LPS is part of the outer membrane of Gram-negative bacteria, the concentration in myxobacterial vesicles seems to be exceptionally low, as confirmed in literature.[34–36] In our hands, the low LPS concentration of SB-OMVs reduces the risk of an unwanted immune reaction.

We further expanded the immunogenicity assessments by incubating primary human immune cells isolated from whole blood with both vesicles at different dilutions. Peripheral blood mononuclear cells (PBMCs) consist of lymphocytes (T-, B-, and NK-cells), monocytes or dendritic cells, which are primarily involved in the innate immune response,[37] and respond to pathogen associated molecular patterns. Activation by those molecules induces fever and swelling, which can finally lead to a septic shock.[38] Here, we quantified cytokines produced by activated immune cells, which are part of the innate immune system, such as IL-6, IL-8, IL-1 beta and tumor necrosis factor (TNF). Vesicles induced a moderate to low release of pro-inflammatory cytokines compared to a 1 μg mL^{-1} positive LPS control (**Figure 1**a–c). The low release of IL-1 beta by RO-EVs, SB-OMVs, and LPS can be explained with a second pathway of cytokine production. The activation of the inflammasome by different caspases cannot be accomplished by LPS, thus the subsequent processing of IL-1 to IL-1 beta was not as abundant.[39]

Based on these findings we were interested to assess whether cytokine release was induced by activation of pattern recognition receptors that normally detect bacterial and exogenous stimuli. We thus tested the activation of toll-like receptors in reporter cells upon incubation with various EV concentrations, as it was previously shown that these specific cells are excellent tools to study EV-mediated interactions.[40] As mentioned above, toll-like receptors respond to pathogen-associated molecular patterns and are an important part of the innate immune system.[41] For SB-EVs, we saw a dose-dependent activation of the toll-like receptor 2 but none for toll-like receptor 4 (Figure S4, Supporting Information). These data extend and support the negative results of the gel clot assay, as toll-like receptor 4 is mostly activated by LPS, while toll-like receptor 2 has a broad recognition pattern of microbial compounds.

We carried our biocompatibility assessments forward in vivo and monitored the toxicity of SB-OMVs and RO-EVs in a *D. rerio* (zebrafish) larvae model. These models provide the opportunity to study the toxicity, efficacy and biodistribution of nanoformulations, allowing for real-time evaluations.[42] We first added ≈10^{11} vesicles to the medium in which the one day post-fertilization (1 dpf) and three days post fertilization (3 dpf) larvae were kept, and used PBS, which is also the eluent of vesicles after SEC, as a control. The amount of PBS, 25% total volume, was limited by the amount zebrafish larvae tolerated (Figure S11, Supporting Information). The development of the larvae was checked each day and monitored for abnormalities regarding heart rate, motor function, pigmentation, and overall appearance of the fish. Until 5 dpf, the development of larvae exposed to SB-OMVs and RO-EVs was not impaired or changed at any time (**Figure 2**). In comparison, it was shown that bovine milk-derived EVs reduced the survival of zebrafish larvae when exposed to EVs in water with comparable concentrations.[43] In that work, altered hatching behavior due to tetraspanin destabilization of the chorion was observed as well. In our study, the hatching rate was similar to controls with no delay nor premature hatching (data not shown). To further increase the exposure of vesicles to the larvae, we injected 1.5 nL with ≈10^6 vesicles into the blood island, mimicking a systemic administration. Even under these conditions, the larvae were not affected. (Figure 2).

2.3. Understanding the Vesicles' Behavior Using an Advanced Three-Dimensional Cell Culture Model and Biodistribution In Vivo

Based on our in vivo results, we wanted to take a step back and better understand the vesicle interaction at the cellular level. Indeed, literature reports on cellular uptake of EVs and OMVs are primarily studying individual cell lines. Cancer cells, for example communicate with stromal cells via EVs through which efficient uptake is required.[44] To analyze the vesicles' behavior, we developed a complex three-dimensional cell culture model.[45] Due to their well-controlled conditions, advanced cell culture models, are helpful in predicting in vitro–in vivo correlations for a better assessment of therapeutic efficiency and safety.[46–48] Our 3D co-culture model was composed of three cell types, namely epithelial cells (CaCo-2) and two immune cell types, macrophage-like cells (*d*THP-1) and dendritic-like cells (MUTZ-3). CaCo-2 cells were used to form the epithelial barrier while the sub-epithelial immune cell types mimic inflammatory responses and present a model of the innate immunity within the epithelial context. In this model, cells were imaged after day 6 (leaky barrier condition) and day 11 (tight barrier condition), mimicking inflammation-related pathophysiology and healthy intestinal physiology, respectively. LPS was applied in both conditions to mimic an acute inflammation, leading to four different scenarios: a leaky epithelial barrier i) with inflammation and ii) without inflammation, and a tight epithelial barrier iii) with inflammation and iv) without inflammation. (**Figure 3**).

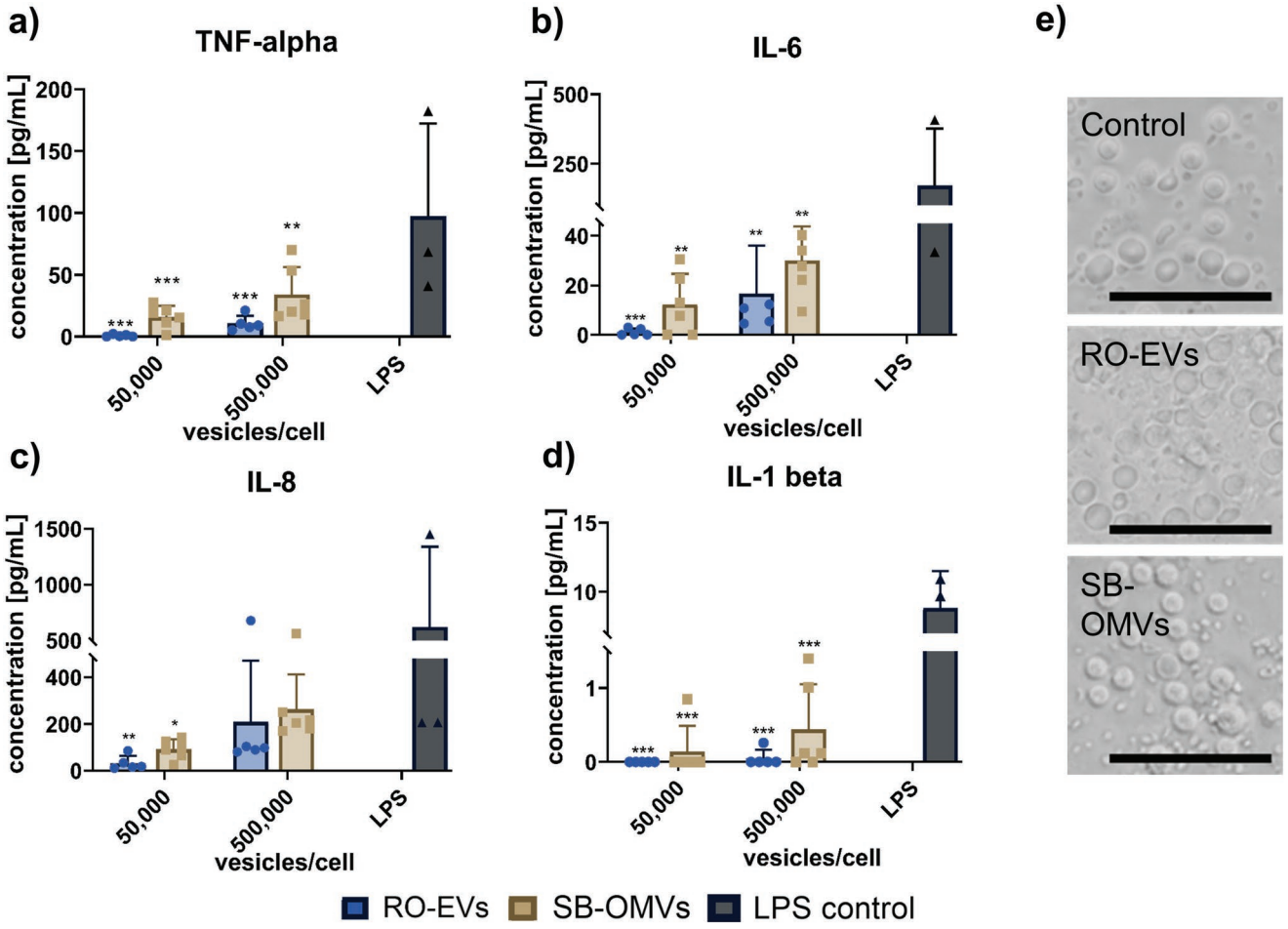

Figure 1. Cytokine release of PBMCs incubated with RO-EVs and SB-OMVs. a) Quantification of TNF after an incubation of PBMCs with RO-EVs, SB-OMVs, and a LPS control (1 µg mL^{-1}) for 4 h. b) Quantification of IL-6, c) IL-8, and d) IL-1 beta. Untreated cells cultured in medium showed cytokine releases of TNF = 0 pg mL^{-1}, IL-6 = 0 pg mL^{-1}, IL-8 = 9.4 ± 7.4, and IL-1 beta = 0 pg mL^{-1}. e) Micrographs of PBMCs after vesicle exposure or control. Concentrations are given in number of vesicles per cell, scale bar 50 µm; n = 3–6, n_{donor} = 3–4.

We incubated the co-culture model for 24 h with DiI fluorescently labelled vesicles, fixed and stained the cells and analyzed them using confocal laser scanning microscopy. During all experiments the barrier function of the epithelial layer was not affected by the vesicles (Figure S5, Supporting Information), which has also been seen in literature.[49] **Figure 4** shows confocal side view images for all four conditions, including leaky and tight barrier, and with and without inflammation. Only

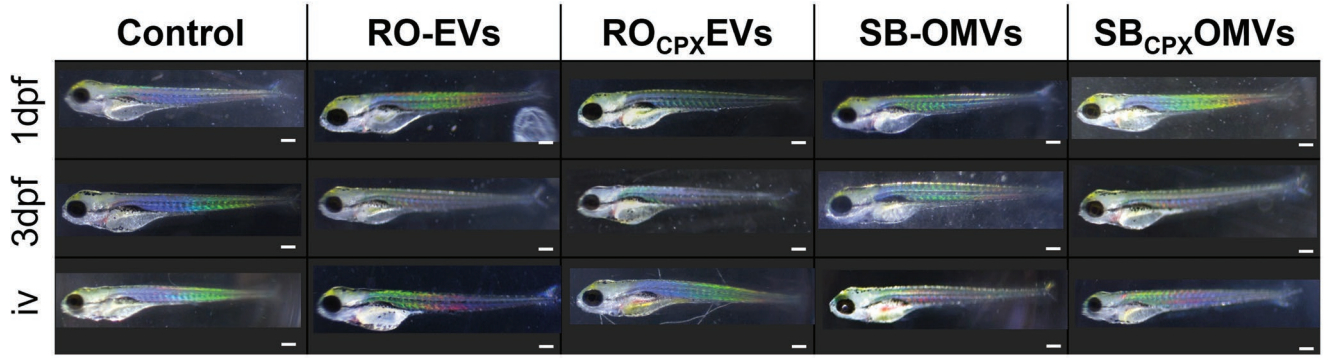

Figure 2. Biocompatibility evaluations of bacterial and mammalian vesicles in vivo. *Danio rerio* larvae were exposed to SB and RO vesicles with ≈10^{11} vesicles at 1 day post-fertilization (dpf) or 3 dpf and kept until 5 dpf without exchanging the water. To increase the exposure, ≈10^{6} SB and RO vesicles were injected into the blood island at 1 dpf. Representative images of 5 dpf larvae. Scale bar 200 µm.

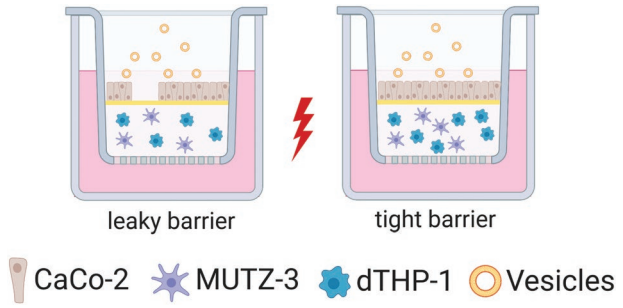

Figure 3. Schematic illustration of the three-dimensional gastrointestinal (GI) co-culture model. CaCo-2 epithelial cells were added on top of a collagen layer containing both immune cell types, MUTZ-3 and dTHP-1, placed in a Transwell system. While the "leaky" barrier model was cultured for 6 days to take advantage of a sub-confluent leaky epithelial layer, the "tight" barrier was cultured until a firm monolayer was established. Under both conditions, an inflammation was simulated by addition of LPS. Fluorescently labeled vesicles were added for 24 h, respectively. Created with BioRender.com.

for the tight model conditions, we observed a high and evenly accumulation of vesicles in the epithelial cell layer. This effect was independent of LPS stimulation and inflammatory state. In the leaky barrier model, vesicles were able to penetrate through the collagen layer, reaching the sub-epithelial immune cells, in particular for SB-OMVs (Figure S6, Supporting Information). When embedding *d*THP-1 macrophage-like cells in a collagen-based monoculture setup (Figure S7, Supporting Information), we observed vesicle uptake for SB-OMVs and for RO-EVs. Interestingly, no uptake of vesicles was observed in dendritic-like cells cultured in collagen monoculture (Figure S8, Supporting Information). These findings indicate that macrophages may be involved in vesicle recognition.

In literature, OMVs derived from *Streptococci* showed increased uptake in dendritic and keratinocyte cells, but comparably minor uptake in macrophages.[50] To the best of our knowledge, the uptake of vesicles has not been investigated in co-culture models including different cell types embedded in a physiologically relevant extracellular matrix. Our model gives better insights into the interaction of EV with epithelial and immune cells, aiding the correlation between in vitro and in vivo. Visualizing the localization of RO-EVs and SB-OMVs in this in vitro co-culture model indicates the potential behavior of these vesicles encountering under healthy conditions or during an infection with concomitant inflammation. The accumulation of the vesicles in the epithelial barrier may be advantageous for targeting *Shigella* because their main replication site is in the epithelial layer.[16] Furthermore, the investigation of the localization of vesicles in the leaky model shows that the vesicles are able to permeate through a compromised epithelial barrier and can be taken up by immune cells under diseased conditions.

In a next experiment, we returned to our zebrafish model to analyze the biodistribution of the vesicles. By measuring the uptake behavior in vivo, we aimed to provide a complete picture of the biogenic carrier's behavior. For this, DiI labeled vesicles were injected into the blood island of 1 dpf larvae, and imaged 2 and 24 h later using confocal scanning microscopy. Two hours after injection, the red signal of the fluorescent vesicles was clearly observed in the tail area of injection (**Figure 5**a). Larvae that were injected 24 h before however, showed that vesicles also located close to the head and further upstream in the main blood supply (Figure 5b). Compared to other nanoparticles, we were not able to see any accumulation in specific organs such as the eye.[51] Based on our results from the three-dimensional cell culture model, we suspect that epithelial cells or macrophages also took up the vesicles, as these have been shown to be central in EV uptake in zebrafish.[52] As seen in Figure 5b, individual cells that were mobile were detected with red vesicle-associated fluorescence. Such findings may indicate the involvement of macrophage cells in vesicle interaction. Overall, our three-dimensional cell culture model in combination with in vivo biodistribution studies contributes to an early stage understanding of cellular interactions of vesicles.

2.4. Encapsulation of Model Antibiotic into Vesicles

The clinical challenge of antimicrobial resistance makes it highly desirable to explore EVs as potential carriers for established antibiotics. To the best of our knowledge, only one example of exogenous loading of antibiotics into EVs is present in literature. Yang et al. loaded linezolid into RAW264.7 EVs via passive incubation and tested them on intracellular *Staphylococcus aureus*.[53] While the concept is interesting and relevant, the authors claimed that unencapsulated drug was removed by a 10 min centrifugation at 10000 × *g*. According to common EV purification practice,[2] such low centrifugal speed and short time period may not be sufficient to completely remove residual free compounds. In our work, we used ciprofloxacin (CPX) as a model antibiotic to be encapsulated into RO-EVs and SB-OMVs. There is increased evidence of resistance development of this broad-spectrum antibiotic, accentuating the urgent need to introduce better application avenues for targeted therapy.[20,54] Four different loading techniques were used to encapsulate CPX into vesicles: i) passive incubation, ii) saponin-assisted, iii) electroporation, and iv) a combination of passive and saponin-assisted loading, all previously described.[55,56] To remove non-encapsulated drug, SEC was the optimal method compared to other commonly used practices (Figure S9, Supporting Information). Loading of vesicles influenced the particle concentration of RO-EVs only, but not to a very high extend compared to the unloaded control group (Figure S10, Supporting Information). The most efficient loading was achieved by passive incubation with 70 ng CPX and 50 ng CPX per 10^{-12} vesicles from RO and SB, respectively (**Figure 6**).

Indeed, passive incubation appears to be one of the preferred methods when it comes to loading small molecules.[57–59] The encapsulation efficiency, however, can be increased for hydrophilic drugs using saponin as mild detergent.[56,59] CPX has an intermediate lipophilicity and the saponin-assisted method did not increase encapsulation efficiencies significantly compared to passive approach. Combining passive incubation with the saponin method increased the encapsulation efficiency of CPX 1.4 times for SB-OMVs but reduced the amount CPX loaded into RO-EVs compared to passive incubation alone. Electroporation was the method with the lowest encapsulation efficiency with 49 ng CPX and 18 ng CPX per 10^{-12} vesicles from RO and SB, respectively. Electroporation was shown to induce

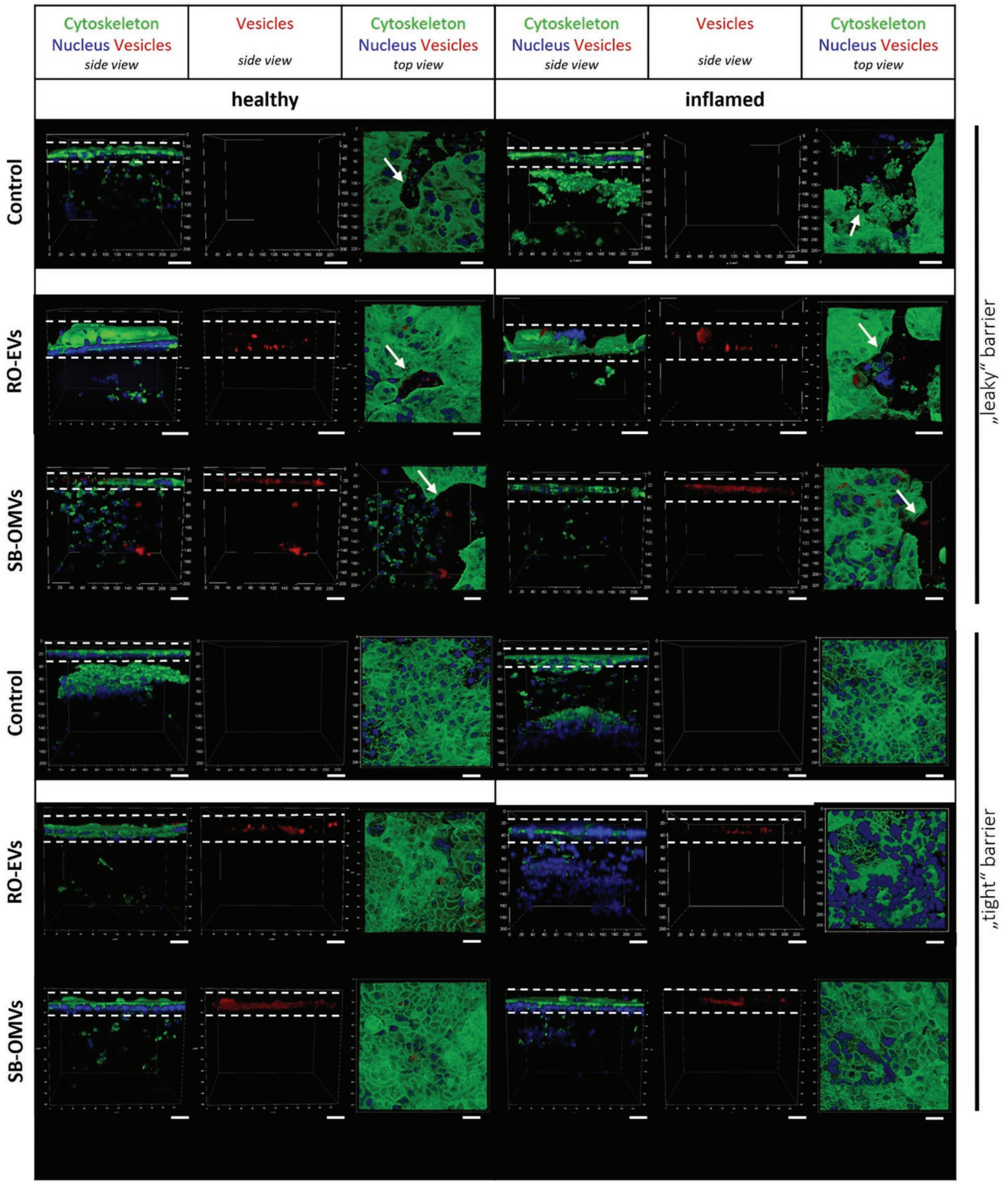

Figure 4. Confocal images of the co-culture model with a leaky (top) and tight (bottom) epithelial barrier. The cytoskeleton was labeled using phalloidin-FITC and is represented in green. Cell nuclei were stained with DAPI (blue) and vesicles labeled with DiI, seen in red. Recorded *z*-stacks of around 300 µm depth are represented in side view and in top view with overlaid fluorescence signal or split channel for DiI-labeled vesicles. White arrows highlight holes in the epithelial layer. White dashed lines frame the epithelial layer. Scale bar 50 µm.

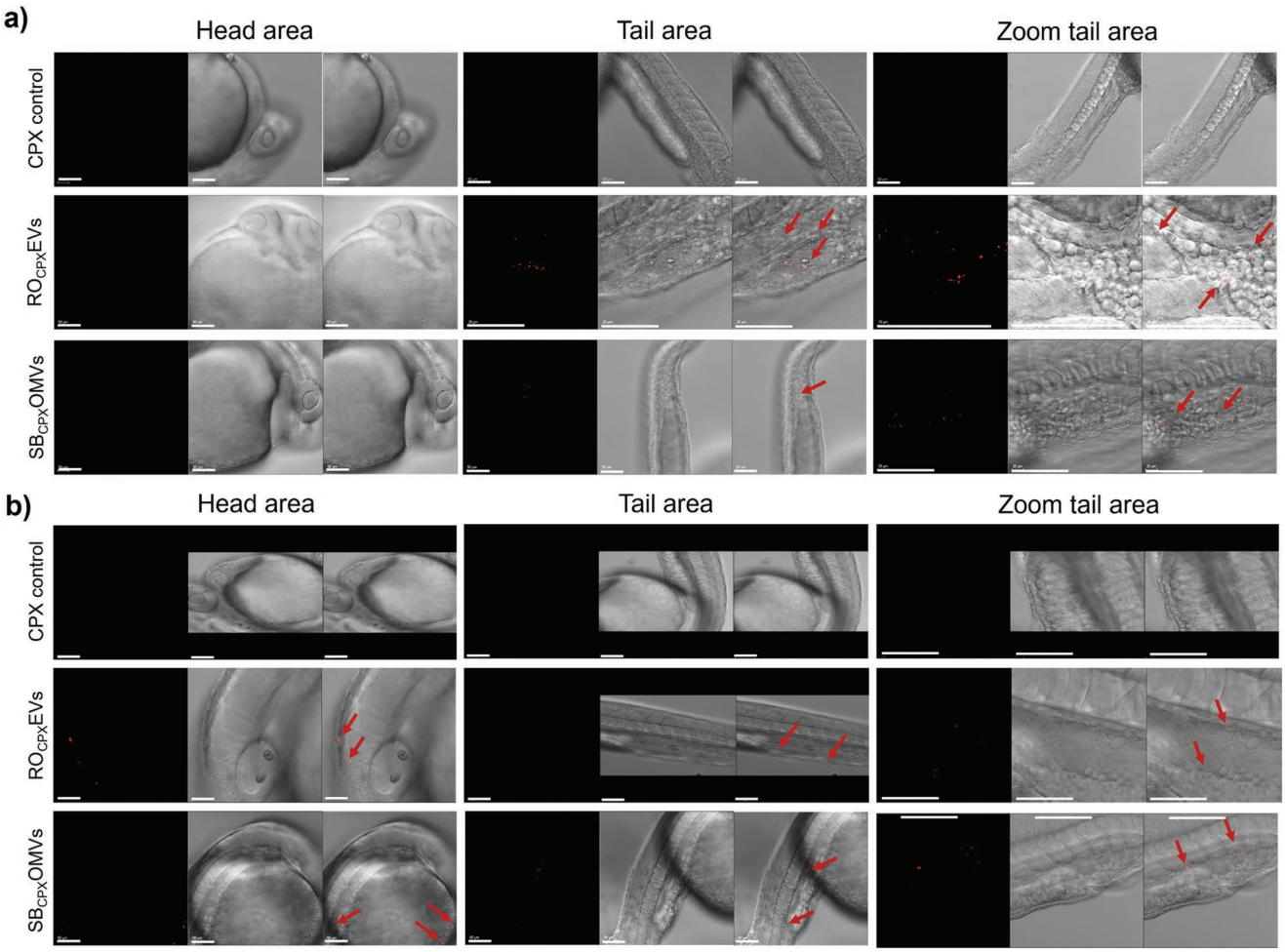

Figure 5. Biodistribution of labeled RO-EVs and SB-OMVs in *Danio rerio* larvae a) images of different larvae after 2 h post-injection and b) after 24 h. Scale bar 100 µm.

precipitation of large molecules[56,60,61] but we did not detect any evidence of precipitation in cryoelectron microscopy images (**Figure 7**). Thus, the majority of the drug seems encapsulated inside the vesicles and not bound to the surface because the zeta potential of both vesicle types did not substantially change upon loading (Figure S10a, Supporting Information).

We have previously shown that the zeta-potential and the composition of the vesicle plays a role in loading efficiency.[56] Indeed, RO-EVs typically had lower zeta-potential, but higher associated protein concentrations (Figure S2, Supporting Information), which may be linked to a higher CPX loading.

2.5. Antimicrobial Evaluations of Ciprofloxacin Loaded Vesicles In Vitro and In Vivo

The CPX loaded vesicles were subsequently tested on *S. flexneri*. At present, gastrointestinal infections caused by *Shigella* spp. show increasing incidence of antimicrobial resistance, especially against CPX.[62,63] We observed that independent of the loading method, both vesicles were able to decrease the growth by at least 1.2 and at most 4.1 log units mL^{-1} (**Figure 8**a,b). Interestingly, at comparable CPX concentrations, SB-OMVs induce a much more profound reduction in the number of colony forming units (Figure 8c). Using the most abundant SEC fraction with particle concentrations higher than 10^{12} vesicles mL^{-1}, the growth reduction was significant with a reduction down to 53% for SB_{CPX}OMVs and 77% for RO_{CPX}EVs (Figure 8d). Whether this may be due to a more efficient way of delivering the drug to the pathogen, can only be speculated.

Although, the mechanism of EV and OMV uptake in eukaryotic cells has been studied intensively, pointing out several uptake mediated mechanisms, there is little known on the specific mechanisms of EV and OMV uptake in bacterial cells.[64] Most likely, their uptake is fusion-mediated, which was demonstrated by Kadurugamuwa et al. where OMVs derived from *Pseudomonas aeruginosa* rapidly fused with *S. aureus* and *Escherichia coli* and confirmed by Zusheng et al.[65,66] LPS may play a role in outer membrane recognition via cell surface proteins.[67] Moreover, evidence from liposomal studies lead to the conclusion that membrane composition plays a role in the efficiency of fusion with bacteria.[68] In our study, two mechanisms, potentially simultaneously influence the uptake and efficacy of SB_{CPX}OMVs in *Shigella*: i) LPS mediated fusion of OMV

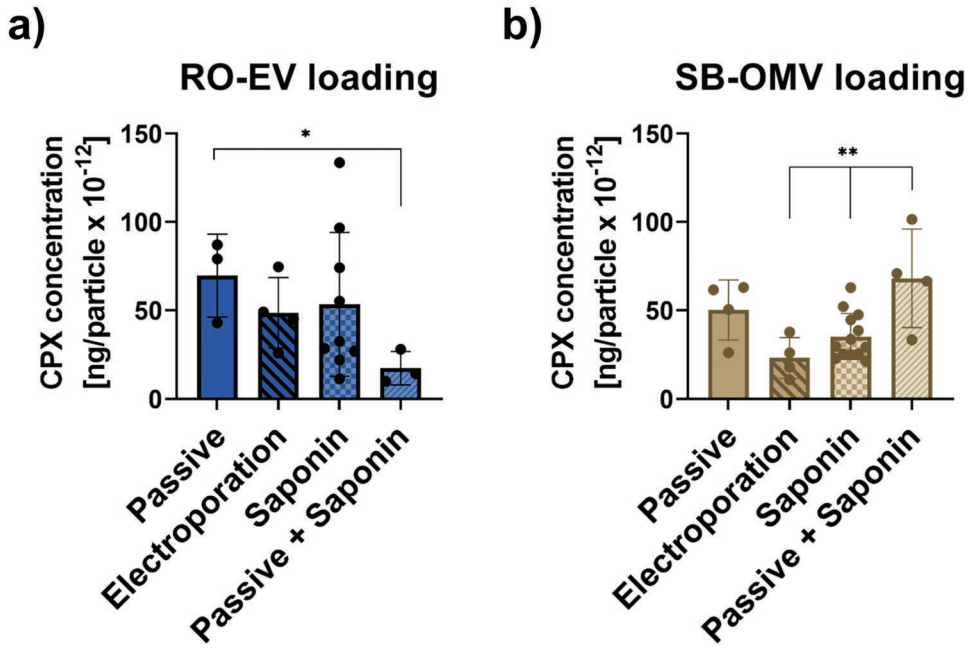

Figure 6. Loading of RO-EVs and SB-OMVs with the model antibiotic CPX. a) CPX loading efficiency of RO-EVs, b) loading efficiency of SB-OMVs using various encapsulation methods. $n = 3–9$, mean ± SD.

with outer membrane components of *Shigella*, and ii) similarities in outer membrane composition between OMVs and *Shigella* facilitating their uptake via fusion. This could explain a more efficient uptake and improved antibiosis of the loaded SB_{CPX}OMVs.

Using our established *D. rerio* model, we first tested the CPX-loaded vesicles for toxicity. When adding EVs to the water or injecting them, survival rates were always at 100% (Figure 2). However, we observed >7% heart edema in fish that were injected with drug-loaded RO_{CPX}EV (≈172.6 ng mL^{-1} CPX) and SB_{CPX}OMV (≈127.8 ng mL^{-1} CPX) (**Figure 9**a,b). Incidences of heart edema due to free CPX injection were nevertheless higher with 13% for 200 ng mL^{-1} and 17% for 150 ng mL^{-1}. When comparing only SB_{CPX} with CPX 150 ng mL^{-1}, a significant reduction of these side effects was observed. For RO_{CPX}, a substantial reduction in toxicity was seen ($p = 0.09$), and it must be noted that these vesicles had more CPX loaded. Toxicity effects were thus induced by CPX because native EVs did not induce any abnormality, indicating high biocompatibility. Although CPX has already been tested in zebrafish larvae, the exact mechanism on cardiotoxicity has not been assessed yet.[69] The development of the heart is a complex process involving a variety of regulatory gene expressions.[70] In our hands, encapsulating CPX into RO-EVs and SB-OMVs reduced its risk for cardiotoxicity, pointing to a beneficial role of vesicles for the clinical application of fluoroquinolones.

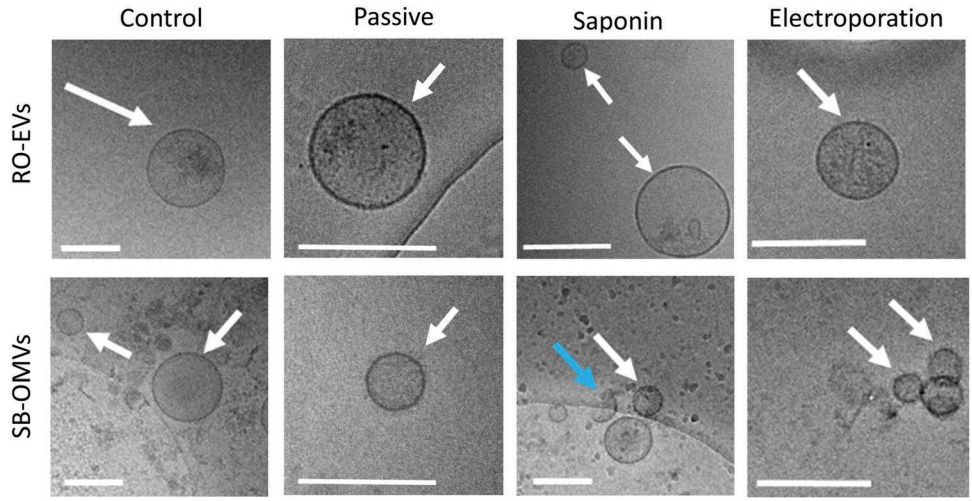

Figure 7. Cryoelectron microscopy images of native and loaded RO-EVs and SB-OMVs. White arrows indicate intact vesicles. The blue arrow indicates a disrupted membrane. Scale bar 200 nm.

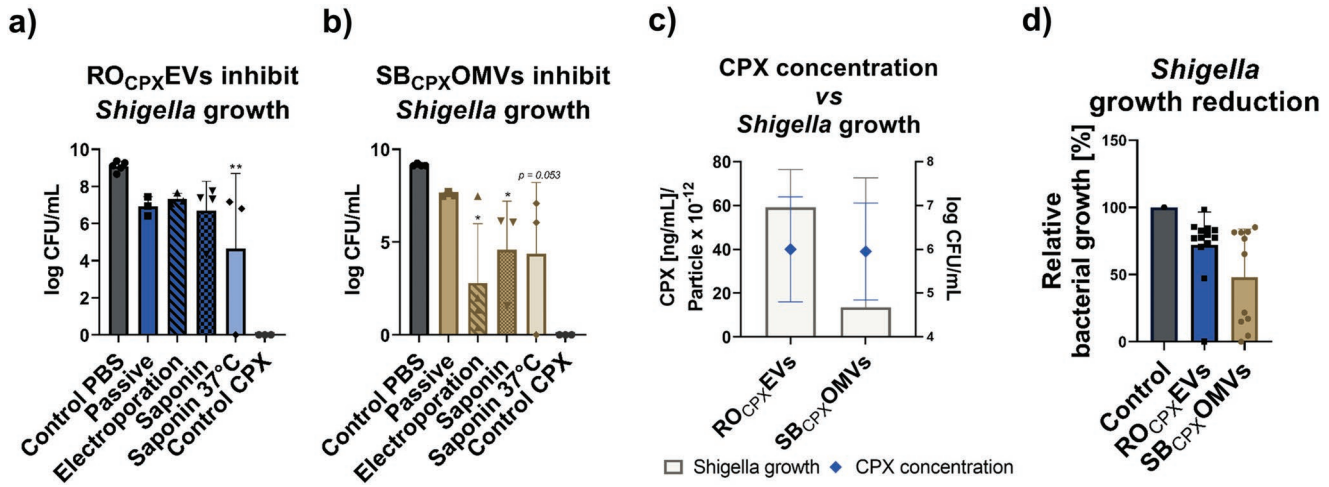

Figure 8. Growth inhibition of RO_{CPX}EVs and SB_{CPX}OMVs depending on their particle concentration. a) Growth inhibition of *Shigella flexneri* after an overnight exposure of undiluted fraction of RO_{CPX}EVs with 1.8e12 ± 7e11 vesicles mL^{-1}. b) Growth inhibition after SB_{CPX}OMV incubation with 3e12 ± 1e12 vesicles mL^{-1}. c) CPX concentration (blue dots) versus colony forming units (white bars) of *S. flexneri* after an overnight incubation with the vesicles. d) Relative bacterial growth after RO_{CPX}EVs, SB_{CPX}OMVs at the highest vesicle concentration compared to PBS control incubation. Mean ± SD, $n = 5$.

In order to evaluate the antibiotic efficiency of the loaded vesicles in vivo, we again, took advantage of our zebrafish larvae model and established an infected version. The purpose of this model was to see if any antimicrobial effect of the vesicles against *Shigella* can be detected in vivo. In literature, it is established that *Shigella* injected into zebrafish larvae leads to infected macrophages and neutrophils, which escaped cytosolic digestion and progressively spread through the entire fish, mimicking a sepsis.[71] Prior to this, we evaluated the tolerated concentration of PBS and CPX in the water of the larvae to define the therapeutic dose, which could be applied with the vesicles (Figure S11, Supporting Information). Next, we established our model by injecting *S. flexneri* GFP into the blood island of 1dpf larvae to mimic a severe systemic infection. With 6.6×10^4 CFU per injection, a stable and persistent infection was generated that allows visual observation of the bacteria in vivo. At this pathogen concentration, larvae survived for 72 h post infection and reached concentrations of up to 7.6 log CFU mL^{-1} per larvae (**Figure 10**a). 4 h after injection, *Shigella* were already detectable by fluorescence microscopy. Subsequently, CPX-loaded RO-EVs were injected into the larvae (Figure 7c). Qualitatively, it was difficult to compare the reduction in *Shigella* fluorescence after 20 h because of unequal exposure times, but EVs may have an influence on the spread of pathogens. When looking at the survival rates, this effect was not clearly identifiable (Figure 10b). Control experiments with similar concentrations of free CPX led to comparable results. To better understand these observations, we performed additional control experiments with free CPX to find out which drug concentration was needed for a complete eradication of the *Shigella* infection.

When using free CPX, only very high concentrations of up to 1000 × MIC values—corresponding to 200 µg drug mL^{-1}—were able to eradicate bacteria when given 4 h after larvae infection. However, at such high concentrations CPX-induced heart edema became substantially more frequent (Figure S12, Supporting Information). Interestingly, the treatment of infected zebrafish in general seems to carry its difficulties also in other infection models.[72,73] For our drug-loaded vesicles, we suspect a reduction in initial *Shigella* growth but because of rapid pathogen spreading throughout the entire larvae, full eradication was challenging. In the future, other models such as a *Staphylococcus aureus* infection in zebrafish may be more suitable to evaluate the therapeutic effect of the vesicles.[74]

3. Conclusions

In this work, we were interested in better characterizing biogenic vesicles in an infection setting. We introduced vesicles derived from B-lymphoid cells and non-pathogenic myxobacteria and efficiently loaded them with ciprofloxacin, an important representative of the fluoroquinolone antibiotic class. Loading into vesicles reduced drug-associated toxicity, which has been observed for the free drug in our in vivo model. Although different attempts in designing vesicle-based antimicrobial carrier system have been presented in literature,[53,75,76] our vesicles have additional advantages, such as ease of production and biocompatibility. The scale up production of the producer cells may be conducted in small fermenters with standard media, leading to economically friendly production and sustainability. When evaluating their immunogenic potential, especially RO-EVs showed promising biocompatible results due to their origin from cells expressing no MHC class II molecules.[28] Through the combination of different simple and complex in vitro models with in vivo evaluations in zebrafish larvae, we established a useful tool assess different vesicle formulations. In our case, we showed that CPX-loaded vesicles are able to kill pathogens in bacteria, but the in vivo infection model needs careful evaluation. An improved encapsulation efficiency might result in increased antibiotic effect in vivo, which could be detected via fluorescence microscopy. Further, a *Shigella* infection model in a different animal could also help to understand the antibiotic effect of the loaded vesicles. The integration of a three-dimensional cell model allowed better

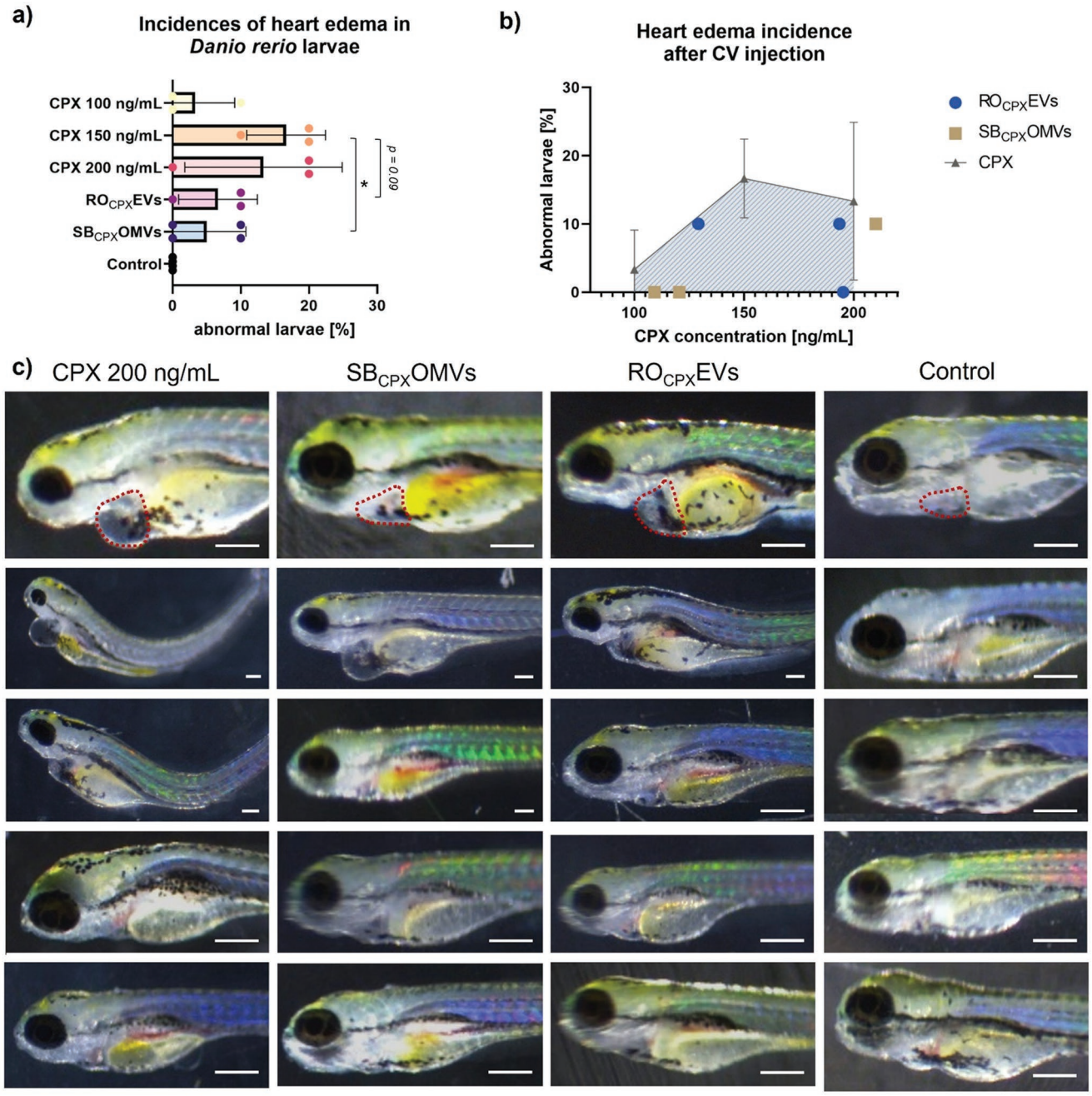

Figure 9. Cardiotoxic effect of CPX and loaded vesicles. a) Percentage of incidences of heart edema development in zebrafish larvae after free CPX, RO_{CPX}EV (≈172.6 ng mL^{-1} CPX) or SB_{CPX}OMV (≈127.8 ng mL^{-1} CPX) injection. *$p = 0.05$ *t*-test; selected individual comparison of RO_{CPX} versus CPX 150 ng mL^{-1}, and SB_{CPX} versus CPX 150 ng mL^{-1}. b) Percentage of development of heart edema compared to CPX concentration, free or encapsulated into vesicles. Individual dots represent individually loaded vesicles with CPX concentration and the percentage of abnormal larvae. The blue area is the area under the number of abnormal larvae due to CPX injection. c) Microscopic images of healthy and abnormal larvae 4 days after injection. The red-dashed line frames the pericardium. Scale bar 200 µm. $n = 10$, $n = 3$–4.

understanding of vesicle accumulation in different cell types, which could be confirmed in the precluding *D. rerio* assessments. We believe that our findings need subsequent formulation efforts to further develop the EV carrier systems. The various models to mimic and predict conditions that biogenic vesicles will encounter should in the future contribute to the clinical translation of these nanoparticles.

4. Experimental Section

Bacterial and Cell Culture: SBSr073 were cultured as previously described, isolating OMVs after 7 days of culturing.[4,29] The composition of this 2SWT medium was 0.3% bacto tryptone, 0.1% soytone, 0.2% glucose, 0.2% soluble starch, 0.1% maltose monohydrate, 0.2% cellobiose, 0.05% $CaCl_2$ $2H_2O$, 0.1% $MgSO_4$ $7H_2O$, and 10 mM HEPES, pH 7.0 adjusted with KOH. *Shigella flexneri* M90T (DSM 4782, DSMZ)

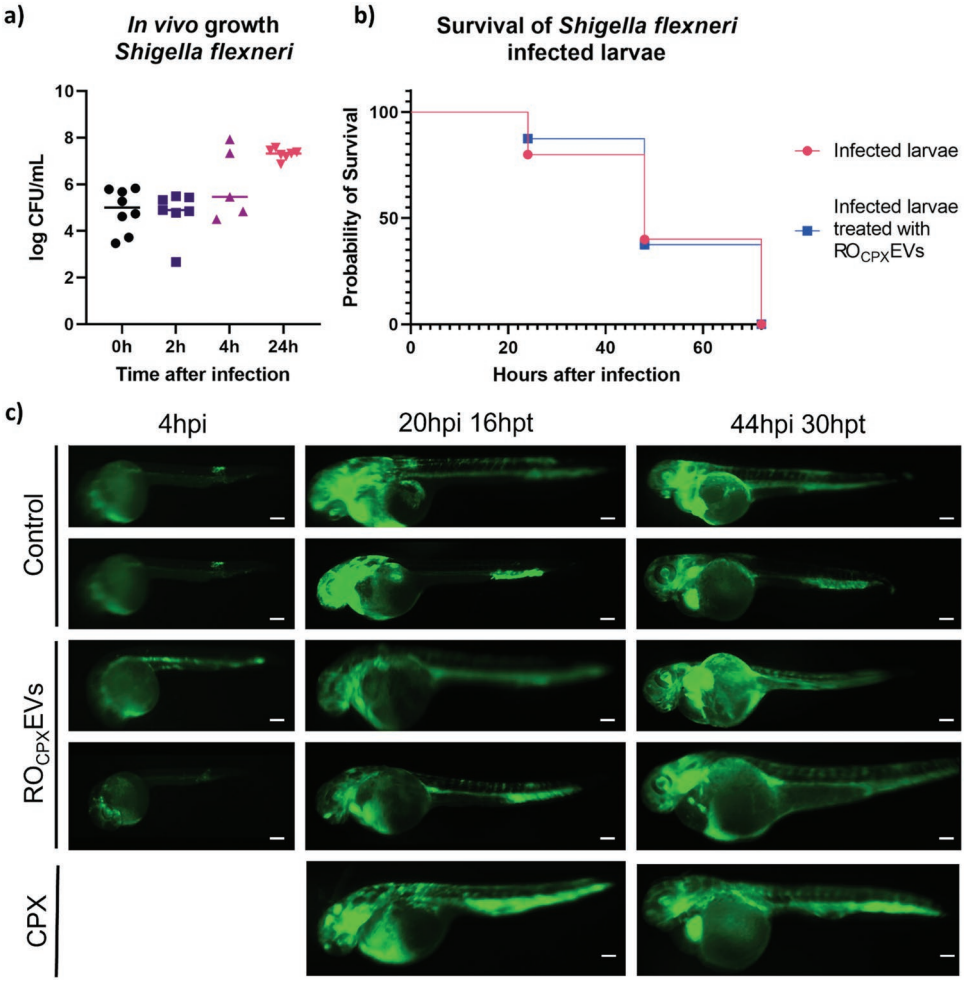

Figure 10. Zebrafish *Shigella* infection model. a) In vivo growth of *S. flexneri* in zebrafish larvae 0, 2, 4, and 24 h after injection. $n = 5–8$. b) Survival of *Shigella* injected larvae. $n = 8–10$. c) Fluorescence microscope images of *Shigella* GPF infected larvae. After 4 h post-infection, larvae were treated by RO_{CPX}EV injection. Controls did not receive any treatment. Scale bar 200 µm.

was cultured in tryptic soy broth (Thermo Fisher) at 37 °C or on tryptic soy agar (Thermo Fisher) at 30 °C. *Shigella flexneri* GFP (ATCC 12022GFP) was cultured in nutrient broth or agar (Thermo Fisher) with 100 µg mL^{-1} ampicillin (Carl Roth).

RO cells (DSMZ, ACC 452) were cultivated in RPMI 1640 (Gibco, Thermo Fisher, Germany) with 1% (v/v) insulin-transferrin-selenium-ethanolamine (Thermo Fisher) as previously described.[29] Briefly, cells were inoculated with a density of 0.75×10^6 cells with a total volume of 45 mL medium in an upright T75 flask. After 4 days, cells were maintained by exchanging 25 mL cell culture supernatant with 50 mL new medium.

CaCo-2 HTB37 (DSMZ, 169) was cultured in DMEM (Gibco) with 1% (v/v) non-essential amino acids (Thermo Fisher) and 10% (v/v) fetal calve serum (FCS). THP-1 (DSMZ, ACC16) grew in RPMI with 10% (v/v) FCS. MUTZ-3 (DSMZ, ACC 295) were cultured in alpha-MEM (Gibco) with 20% FCS.

Vesicle Purification and Characterization: Vesicles were isolated as recently described.[4,29] Briefly, 100 mL of $\approx 7 \times 10^6$ cells mL^{-1} RO cell supernatants were centrifuged at $300 \times g$ for 8 min, 100 mL SBSr073 supernatants at $9500 \times g$ for 10 min. Subsequently, both vesicle supernatants were centrifuged at $9500 \times g$ for 15 min. Vesicles were isolated by differential centrifugation at $100\,000 \times g$ for 2 h at 4 °C using a rotor type 45 Ti with a *k* factor of 133 at maximum speed (Beckman Coulter). Both pellets were suspended in 500 µL residual supernatant. They were purified using size-exclusion chromatography.[4,29] To obtain equivalent particle concentrations, 390 mL of conditioned RO medium compared to 65 mL of conditioned SBSr073 medium had to be obtained for vesicle isolation because myxobacteria produce higher yields of vesicles per cell.[4,56]

Particle concentrations were measured using nanoparticle tracking analysis. With a camera level of 15, a detection threshold of 5 and 20 to 120 particles per frame. The size and concentration were calculated using the NanoSight 3.3. software. The zeta potential was measured using the Zetasizer Nano (Malvern) and folded capillary cells (Malvern), analyzed with Zetasizer software 8.01.4906. Protein concentrations were conducted using a bicinchoninic assay kit (Sigma Aldrich) according to manufacturer's specifications. Surface markers CD9 and CD63 were analyzed using a bead array kit and flow cytometry detection (BD Bioscience). Isotype antibodies were used as negative control.

For cryo-electron microscopy 3 µL of the vesicles dispersion was vitrified to a thin electron transparent sample using a Gatan CP3 cryo plunger operating at –165 °C. Then the sample was transferred to a Gatan model 914 cryo-TEM sample holder under liquid nitrogen. TEM bright field images at low dose conditions were acquired at –170 °C and 200 kV accelerating voltage. Therefore a JEOL JEM-2100 LaB_6 transmission electron microscope equipped with a Gatan Orius SC1000 CCD camera was used.

Gel Clot Endotoxin Detection: Vesicles were isolated as described and under aseptic conditions. After determining the particle concentration, a gel clot assay (Toxin Sensor Endotoxin detection system, GenScript) was

performed according to manufacturer's specifications with two different dilutions of the vesicle pellet, LAL reagent water and an *E. coli* endotoxin standard. A positive reaction was confirmed by a firm gel formation, indicating an equal or higher endotoxin concentration of 0.25 EU mL^{-1}, which is the allowed limit for sterile water for injection according to the federal drug and food administration.

Cytokine Detection of Vesicle Treated PBMC and Reporter Cell Assays: Buffy coats were obtained from three different donors from the Blood Donation Center, Saarbrücken, Germany, under the authorization by the local ethics committee (State Medical Board of Registration, Saarland, Germany; permission no. 173/18). With a seeding density of 100 000 cells per well in a 96 well plate, cells were incubated with either 5×10^5 or 5×10^4 particles per cell for 4 h in RPMI 1640. Cell supernatants were collected and stored at −80 °C until cytokine quantification. To determine IL-6, IL-8, IL-1 beta, and TNF a BD cytometric bead array human inflammatory cytokine kit was used according to manufacturer's specifications. Cytokine quantification and sample analysis was analyzed with FCAP array.

HEK-Dual hTLR2 cells (Invivogen, Toulouse, France; #hkd-htlr2ni) and HEK-Blue hTLR4 cells (Invivogen, #hkb-htlr4) expressing secreted embryonic alkaline phosphatase (SEAP) were used to determine NF-κB/AP-1 activity. Cells were seeded in 96-well plates at a density of 5×10^4 cell per well, and simultaneously treated with either 5×10^5 or 5×10^4 particles per cell of EV samples or liposomes (POPE, POPG, and CL in a 70:20:10 weight ratio) at concentration of 5×10^5 per cell. Ultrapure LPS from *E. coli* K12 (Invivogen, #tlrl-peklps) and Pam3CSK4 (#tlrl-pms) were used at concentration of 10 ng mL^{-1} as positive controls for HEK-TLR2 and HEK-TLR4 cells respectively. After 24 and 16 h of incubation for HEK-Dual hTLR2 and HEK-Blue hTLR4, respectively, 20 µL of cell culture supernatant from each well was mixed with 180 µL of resuspended QUANTI-Blue Solution (Invivogen, #REP-QB2) and incubated at 37 °C for 1–3 h. SEAP activity was measured with microplate reader (PromegaTM GloMax Plate Reader Madison, WI, USA) at 600 nm. To ensure that EVs were non-toxic the MTT colorimetric assay was performed as described previously.[77] Absorbance was measured at 560 nm using a microplate reader (PromegaTM GloMax Plate Reader Madison, WI, USA).

Localization of Vesicles in a Co-Culture Model: The leaky gut model was further based on the previously established co-culture system in the group.[47] In brief, monocytic-THP-1 cells were differentiated into macrophage-like cells (*d*THP-1) using 50 nM phorbol 12-myristate 13-acetate (PMA, Sigma-Aldrich, Taufkirchen, Germany) for 72 h. For co-culture, *d*THP-1 (20 000 per well) and dendritic MUTZ-3 (10 000 per well) cells were embedded in 80% (v/v) collagen type I (3 mg mL^{-1}, PureCol; Advanced Biomatrix, Tucson, USA) solution containing 10% 10X RPMI + 20 mg mL^{-1} $NaHCO_3$ (Gibco) and 10% human AB serum (Sigma). A total volume of 150 µL was placed to the apical chamber of the insert (Transwell Permeable Supports 3460, Corning). After 1 h of solidification at 37 °C and 5% CO_2, epithelial CaCo-2 cells (100 000 per well) were seeded on top, in a total volume of 0.5 mL DMEM with 10% FCS and 1% penicillin/streptomycin (Pen/Strep, Gibco). Afterward, 1.5 mL of RPMI with 10% FCS and 1% Pen/Strep was added to the basolateral side. Cells were cultured under submerged conditions and medium was exchanged every 2 to 3 days. For an inflamed state, the co-culture was stimulated on day 6 (leaky CaCo-2 barrier) or on day 11 (tight CaCo-2 barrier) apically with 10 µg mL^{-1} LPS (Sigma). After 24 h of stimulation, 200 µL on the apical side were removed and 100 µL Vybrant DiI (Thermo Fisher) labeled vesicles were added. Vesicles were labelled according to previous protocols and purified using a 40 mL sepharose CL-2B SEC.[29] After 24 h, cells were fixed with 4% (v/v) paraformaldehyde (Electron Microscopy Sciences), washed, stained with fluorescein phalloidin (Thermo Fisher) and 4',6-Diamidino-2-Phenylindole, Dihydrochloride (DAPI) (Thermo Fisher) according to manufacturer's specifications. Confocal microscope (Leica TCS SB8) images were acquired using the following settings with a 20× objective: DiI (Ex/Em 561 nm/588–609 nm), DAPI (Ex/Em 405 nm/ 420–503 nm), FITC (Ex/Em 488 nm/511–550 nm); 1024 × 1024 pixel. Leica Application Suite X was used to process images.

Loading Vesicles with Ciprofloxacin: After vesicle isolated via ultracentrifugation, the pellet was resuspended in residual supernatant and incubated with 17 mM ciprofloxacin-hydrochloride monohydrate (CPX) (Sigma Aldrich) using the following loading methods. During passive loading, vesicles were incubated with CPX for 30 min at 37 °C. For electroporation, vesicles were mixed with CPX in Gene pulser cuvettes (0.4 cm cell electrode), where settings with 200 Ω, 500 µF and 200 mV with a pulse time of 9–18 ms were used (BioRad Gene Pulser). The saponin-assisted technique was performed by adding 0.1 mg mL^{-1} saponin (Sigma Aldrich) and incubation at RT for 20 min. The combination of passive and saponin was conducted by incubating the vesicles pellet at 37 °C for 30 min with 0.1 mg mL^{-1} saponin. To remove non-encapsulated drug, all samples were purified by a size exclusion chromatography, using a glass column packed with 35 mL of sepharose CL-2B and filtered PBS as eluent. Vesicles typically eluted after 12–15 mL and particle concentrations were determined by nanoparticle tracking analysis. CPX release was measured using mini-Slide-A-lyzer (Life Technologies) with a cut off of 10 kDa. Slide-A-lyzer were placed inside either a solution with a pH of 1 or 7.4. Samples were drawn at consecutive time points from the inside of the dialysis membrane. CPX encapsulation was quantified by Bruker EVOQ TQ Elite ER mass spectrometer coupled with Dionex Ultimate 3000 SL liquid chromatography system. Samples were first mixed with 250 nM cinnaricin and triton-X (0.1% v/v) of which 1 µL was injected into the column. The mobile phase included (A) 0.1% formic acid in ddH2O and (B) 0.1% formic acid in acetonitrile. A linear gradient 5–95% B in A was established for separation on a Waters Acquity BEH C18 column (50 × 2.1 mm, 1.7 µm) for 2.5 min. The flow rate was set to 0.6 mL min^{-1} and column thermostat to 45 °C. LC flow was split to 83 µL min^{-1} before entering the mass spectrometer. The instrument was operated under positive ionization mode with multiple reaction monitoring (MRM) of two transitions for CPX, *m/z* 332 to quantifier ion *m/z* 288 (collision energy −15 V) and to qualifier ion *m/z* 245 (collision energy −22 V). Corresponding source parameters were maintained at 4000 V spray voltage, 150 °C cone temperature, 15 L min^{-1} cone gas flow, 140 °C heated probe temperature, 10 L min^{-1} probe gas flow and 30 L min^{-1} nebulizer gas flow. Samples were analyzed using TASQ 4.0 software.

Growth Inhibition of Shigella flexneri: Bacteria were cultured in liquid conditions until late log or early stationary phase. In order to have similar conditions, *Shigella* was diluted to a final concentration of $2.2 \times 10^5 \pm 9.3 \times 10^4$ CFU mL^{-1}.[78] One hundred milliliter of either loaded vesicles, vesicle dilution, control (sterile PBS), or free CPX was incubated with 100 µL bacterial suspension at 37 °C overnight. Subsequently, colony-forming units were conducted, incubating samples at 30 °C and counted after an overnight incubation.

Zebrafish Husbandry: According to standard operating procedures, AB wild-type zebrafish were raised in Danieau's medium (17 mM NaCl, 2 mM KCl, 0.12 mM $MgSO_4$, 1.8 mM $Ca(NO_3)_2$, 1.5 mM HEPES, 1.2 µM methylene blue at pH 7.1–7.3) with continuous water circulation as described previously.[79]

Toxicity Evaluation and Biodistribution of Vesicles in Zebrafish Larvae: One dpf and 3 dpf larvae were transferred to 96 well plates, with one larva per well and at least 10 larvae per condition. Residual medium was removed and loaded vesicles (25% in Danieau's), free CPX with different concentrations or PBS (25% in Danieau's) as a control added to the well. Each day the moto function, heartbeat, pigmentation, and overall appearance of the fish was monitored using a Stemi 508 KMAT (Zeiss). For the toxicity assessment after injection, 1 dpf larvae were dechorinated with 1 mg mL^{-1} pronase (Sigma), washed in Danieau's and anesthetized with 0.25 mg mL^{-1} tricaine (Sigma). Samples or controls, mixed 1:1 with phenol red (Sigma) were injected into the blood island with a volume of 1.5 nL for a systemic administration, using a FemtoJet Microinjector (Eppendorf). Larvae were washed and transferred to 96 well plates to study toxicity. For the biodistribution assays, vesicles were loaded and labeled with DiI (Thermo Fisher) according to previous protocols.[29] Samples were mixed 10:1 with phenol red and injected into the blood island. Larvae were washed in Danieau's, transferred to chamber slides (ibidi) and embedded in a 1.5% (m/v) low melding

agarose (Thermo Fisher) gel before they were imaged using confocal scanning microscopy. All larvae were sacrificed at 5 dpf.

Development of a Shigella flexneri Model in Zebrafish Larvae: One dpf larvae were dechorinated and anesthetized before they were infected with $6.6 \pm 2.6 \times 10^4$ CFU. Larvae were kept in 0.03 mg mL^{-1} 1-phenyl 2-thiourea (Sigma) in Danieau's. After 4, 24, and 48 h fluorescence microscope (Leica MZ 10 F) images were taken. To conduct the in vivo growth of *Shigella*, larvae were washed twice with 100 µg mL^{-1} ampicillin in PBS and transferred to an Eppendorf tube with one glass bead. Larvae were vortexed for several minutes. The suspension was diluted accordingly and plated on ampicillin nutrient agar plates, where colony forming units were counted the next day.

Statistical Analysis: Data are displayed as mean ± standard deviation (SD) and *n* as the number independent experiments. Statistical analysis was performed by applying One-way ANOVA followed by Tukey or Dunnett post-hoc tests, using SigmaPlot. Significant *p*-values were displayed either as the exact value, * for $p < 0.05$ or ** for $p < 0.01$ or *** for $p < 0.001$.

Supporting Information

Supporting Information is available from the Wiley Online Library or from the author.

Acknowledgements

The authors would like to acknowledge Ronald Garcia for providing SBSr073 myxobacterial cultures, Verena Qallaku for maintaining the zebrafish husbandry and providing fertilized eggs, Susanne Kirsch-Dahmen and Jennifer Herrmann for the support and introduction to the zebrafish facilities. The authors thank Miriam Jaki for her help in determining physicochemical differences between loaded and unloaded vesicles, Mina Mehanny for preparing control liposomes, and Charlotte Dahlem for her help with PBMC isolation. This work was supported by the NanoMatFutur Junior Research programme from the Federal Ministry of Education and Research, Germany (Grant No. 13XP5029A, BEVA). This work received funding from the European Research Council (ERC) under the European Union's Horizon 2020 research and innovation programme (Grant Agreement No. 945602, Gels4Bac).

Open access funding enabled and organized by Projekt DEAL.

Conflict of Interest

The authors declare no conflict of interest.

Author Contributions

E.H. conducted all experiments on RO-EVs, SB-OMVs isolation, characterization, biocompatibility testing and loading, bacterial growth inhibition, zebrafish toxicity assays, zebrafish *Shigella* infection. O.H. established the three-dimensional co-culture and help with confocal imaging. B.L. and C.M.L. supervised the three-dimensional co-culture model. C.W. quantified ciprofloxacin concentrations. M.K. took cryo-electron microscopy images. A.K. conducted and analyzed reporter cell assays. L.P.J. characterized drug-loaded vesicles. A.K.K. and J.H. supervised and revised cytokine detection experiments, and reporter cell assays. R.M. kindly provided myxobacterial strains and zebrafish larvae, and advised on their culture and handling. G.F. received the study, supervised the project, wrote, and revised the manuscript together with E.H. All authors approved the final manuscript text.

Data Availability Statement

The data that support the findings of this study are available from the corresponding author upon reasonable request.

Keywords

B-lymphoid RO cells, ciprofloxacin, extracellular vesicles, myxobacteria, outer membrane vesicles, *Shigella flexneri*, zebrafish larvae

Received: November 30, 2022
Revised: February 17, 2023
Published online: March 20, 2023

[1] G. van Niel, G. D'Angelo, G. Raposo, *Nat. Rev. Mol. Cell Biol.* **2018**, *19*, 213.
[2] C. Théry, K. W. Witwer, E. Aikawa, M. J. Alcaraz, J. D. Anderson, R. Andriantsitohaina, A. Antoniou, T. Arab, F. Archer, G. K. Atkin-Smith, D. C. Ayre, J.-M. Bach, D. Bachurski, H. Baharvand, L. Balaj, S. Baldacchino, N. N. Bauer, A. A. Baxter, M. Bebawy, C. Beckham, A. Bedina Zavec, A. Benmoussa, A. C. Berardi, P. Bergese, E. Bielska, C. Blenkiron, S. Bobis-Wozowicz, E. Boilard, W. Boireau, A. Bongiovanni, et al., *J. Extracell. Vesicles* **2018**, *7*, 1535750.
[3] J. E. Berleman, S. Allen, M. A. Danielewicz, J. P. Remis, A. Gorur, J. Cunha, M. Z. Hadi, D. R. Zusman, T. R. Northen, H. E. Witkowska, M. Auer, *Front. Microbiol.* **2014**, *5*, 474.
[4] E. Schulz, A. Goes, R. Garcia, F. Panter, M. Koch, R. Müller, K. Fuhrmann, G. Fuhrmann, *J. Controlled Release* **2018**, *290*, 46.
[5] E. Woith, G. Fuhrmann, M. F. Melzig, *Int. J. Mol. Sci.* **2019**, *20*, 5695.
[6] A. Latifkar, Y. H. Hur, J. C. Sanchez, R. A. Cerione, M. A. Antonyak, *J. Cell Sci.* **2019**, *132*, 222406.
[7] P. D. Robbins, A. E. Morelli, *Nat. Rev. Immunol.* **2014**, *14*, 195.
[8] S. W. Kim, S. B. Park, S. P. Im, J. S. Lee, J. W. Jung, T. W. Gong, J. M. S. Lazarte, J. Kim, J.-S. Seo, J.-H. Kim, J.-W. Song, H. S. Jung, G. J. Kim, Y. J. Lee, S.-K. Lim, T. S. Jung, *Sci. Rep.* **2018**, *8*, 5402.
[9] S. Fulsundar, K. Harms, G. E. Flaten, P. J. Johnsen, B. A. Chopade, K. M. Nielsen, *Appl. Environ. Microbiol.* **2014**, *80*, 3469.
[10] A. Goes, L. Vidakovic, K. Drescher, G. Fuhrmann, *Nanoscale* **2021**, *13*, 14287.
[11] D.-K. Ho, A. Costa, C. De Rossi, C. de Souza Carvalho-Wodarz, B. Loretz, C.-M. Lehr, *Mol. Pharmaceutics* **2018**, *15*, 1081.
[12] S. Sachetelli, H. Khalil, T. Chen, C. Beaulac, S. Sénéchal, J. Lagacé, *Biochim. Biophys. Acta, Biomembr.* **2000**, *1463*, 254.
[13] A. J. Huh, Y. J. Kwon, *J. Controlled Release* **2011**, *156*, 128.
[14] K. C. S. Browne, R. Chen, M. D. Willcox, D. S. Black, W. R. Walsh, N. Kumar, *Int. J. Mol. Sci.* **2020**, *21*, 7047.
[15] C. J. Graham, *J. Global Health Rep.* **2017**, *1*, e2017002.
[16] D. Philpott, J. Edgeworth, P. Sansonetti, *Philos. Trans. R. Soc., B* **2000**, *355*, 575.
[17] D. J. Philpott, J. D. Edgeworth, P. J. Sansonetti, *Philos. Trans. R. Soc., B* **2000**, *355*, 575.
[18] H. Ashida, H. Mimuro, C. Sasakawa, *Front. Immunol.* **2015**, *6*, 219.
[19] I. J. Azmi, B. K. Khajanchi, F. Akter, T. N. Hasan, M. Shahnaij, M. Akter, A. Banik, H. Sultana, M. A. Hossain, M. K. Ahmed, S. M. Faruque, K. A. Talukder, *PLoS One* **2014**, *9*, e102533.
[20] B. Gu, Y. Cao, S. Pan, L. Zhuang, R. Yu, Z. Peng, H. Qian, Y. Wei, L. Zhao, G. Liu, M. Tong, *Int. J. Antimicrob. Agents* **2012**, *40*, 9.
[21] World Health Organization, Ten threats to global health in 2019.
[22] C. J. L. Murray, K. S. Ikuta, F. Sharara, L. Swetschinski, G. Robles Aguilar, A. Gray, C. Han, C. Bisignano, P. Rao, E. Wool, S. C. Johnson, A. J. Browne, M. G. Chipeta, F. Fell, S. Hackett,

G. Haines-Woodhouse, B. H. Kashef Hamadani, E. A. P. Kumaran, B. McManigal, R. Agarwal, S. Akech, S. Albertson, J. Amuasi, J. Andrews, A. Aravkin, E. Ashley, F. Bailey, S. Baker, B. Basnyat, A. Bekker, et al., *Lancet* **2022**, *399*, 629.
[23] S. Hua, M. B. C. de Matos, J. M. Metselaar, G. Storm, *Front. Pharmacol.* **2018**, *9*.
[24] I. K. Herrmann, M. J. Wood, G. Fuhrmann, *Nat. Nanotechnol.* **2021**, *16*, 748.
[25] R. Poupardin, M. Wolf, D. Strunk, *Adv. Drug Delivery Rev.* **2021**, *176*, 113872.
[26] L. Pourtalebi Jahromi, G. Fuhrmann, *Adv. Drug Delivery Rev.* **2021**, *173*, 125.
[27] T. C. Barrett, W. W. K. Mok, A. M. Murawski, M. P. Brynildsen, *Nat. Commun.* **2019**, *10*, 1177.
[28] C. d. Préval, M. R. Hadam, B. Mach, *N. Engl. J. Med.* **1988**, *318*, 1295.
[29] E. Schulz, A. Karagianni, M. Koch, G. Fuhrmann, *Eur. J. Pharm. Biopharm.* **2020**, *146*, 55.
[30] C. M. Beez, M. Haag, O. Klein, S. Van Linthout, M. Sittinger, M. Seifert, *J. Nanobiotechnol.* **2019**, *17*, 72.
[31] J. D. Cecil, N. M. O'Brien-Simpson, J. C. Lenzo, J. A. Holden, W. Singleton, A. Perez-Gonzalez, A. Mansell, E. C. Reynolds, *Front. Immunol.* **2017**, *8*, 1017.
[32] Department of Health, Education, and Welfare, Public Health Service, Food and Drug Administration Bacterial Endotoxins/Pyrogens, https://www.fda.gov/inspections-compliance-enforcement-and-criminal-investigations/inspection-technical-guides/bacterial-endotoxinspyrogens.
[33] Y. Li, D. Boraschi, *Nanomedicine* **2016**, *11*, 269.
[34] C. Ruiz, A. Ruiz-Bravo, G. A. De Cienfuegos, A. Ramos-Cormenzana, *Microbiology* **1985**, *131*, 2035.
[35] A. J. McBroom, M. J. Kuehn, *Genes Dev.* **2005**, *19*, 2645.
[36] L. J. Shimkets, M. Dworkin, H. Reichenbach, in *The Prokaryotes: Proteobacteria: Delta, Epsilon Subclass*, Vol. *7* (Eds: M. Dworkin, S. Falkow, E. Rosenberg, K.-H Schleifer, E. Stackebrandt), Springer New York, New York, NY, **2006**, pp. 31–115.
[37] C. R. Kleiveland, in *The Impact of Food Bioactives on Health: In Vitro and Ex Vivo Models* (Eds: K. Verhoeckx, P. Cotter, I. López-Expósito, C. Kleiveland, T. Lea, A. Mackie, T. Requena, D. Swiatecka, H. Wichers), Springer International Publishing, Cham, **2015**, pp. 161–167.
[38] J.-M. Zhang, J. An, *Int. Anesthesiol. Clin.* **2007**, *45*, 27.
[39] K. V. Swanson, M. Deng, J. P. Y. Ting, *Nat. Rev. Immunol.* **2019**, *19*, 477.
[40] J. Hoppstädter, A. Dembek, R. Linnenberger, C. Dahlem, A. Barghash, C. Fecher-Trost, G. Fuhrmann, M. Koch, A. Kraegeloh, H. Huwer, A. K. Kiemer, *Front. Immunol.* **2019**, *10*, 1634.
[41] N. J. Gay, M. F. Symmons, M. Gangloff, C. E. Bryant, *Nat. Rev. Immunol.* **2014**, *14*, 546.
[42] S. Sieber, P. Grossen, P. Detampel, S. Siegfried, D. Witzigmann, J. Huwyler, *J. Controlled Release* **2017**, *264*, 180.
[43] A. Matsuda, A. Moirangthem, R. S. Angom, K. Ishiguro, J. Driscoll, I. K. Yan, D. Mukhopadhyay, T. Patel, *J. Appl. Toxicol.* **2020**, *40*, 706.
[44] H. Peinado, M. Alečković, S. Lavotshkin, I. Matei, B. Costa-Silva, G. Moreno-Bueno, M. Hergueta-Redondo, C. Williams, G. García-Santos, C. Ghajar, A. Nitadori-Hoshino, C. Hoffman, K. Badal, B. A. Garcia, M. K. Callahan, J. Yuan, V. R. Martins, J. Skog, R. N. Kaplan, M. S. Brady, J. D. Wolchok, P. B. Chapman, Y. Kang, J. Bromberg, D. Lyden, *Nat. Med.* **2012**, *18*, 883.
[45] O. Hartwig, B. Loretz, A. Nougarede, D. Jary, E. Sulpice, X. Gidrol, F. Navarro, C.-M. Lehr, *J. Controlled Release* **2022**, *345*, 646.
[46] F. Leonard, E.-M. Collnot, C.-M. Lehr, *Mol. Pharmaceutics* **2010**, *7*, 2103.
[47] J. Susewind, C. de Souza Carvalho-Wodarz, U. Repnik, E.-M. Collnot, N. Schneider-Daum, G. W. Griffiths, C.-M. Lehr, *Nanotoxicology* **2016**, *10*, 53.
[48] H. Bouwmeester, J. Poortman, R. J. Peters, E. Wijma, E. Kramer, S. Makama, K. Puspitaninganindita, H. J. P. Marvin, A. A. C. M. Peijnenburg, P. J. M. Hendriksen, *ACS Nano* **2011**, *5*, 4091.
[49] T. Kuhn, M. Koch, G. Fuhrmann, *Small* **2020**, *16*, 2003158.
[50] M. Mehanny, M. Koch, C.-M. Lehr, G. Fuhrmann, *Front. Immunol.* **2020**, *11*, 80.
[51] M. van Pomeren, N. R. Brun, W. J. G. M. Peijnenburg, M. G. Vijver, *Aquat. Toxicol.* **2017**, *190*, 40.
[52] V. Hyenne, S. Ghoroghi, M. Collot, J. Bons, G. Follain, S. Harlepp, B. Mary, J. Bauer, L. Mercier, I. Busnelli, O. Lefebvre, N. Fekonja, M. J. Garcia-Leon, P. Machado, F. Delalande, A. A. López, S. G. Silva, F. J. Verweij, G. van Niel, F. Djouad, H. Peinado, C. Carapito, A. S. Klymchenko, J. G. Goetz, *Dev. Cell* **2019**, *48*, 554.
[53] X. Yang, G. Shi, J. Guo, C. Wang, Y. He, *Int. J. Nanomed.* **2018**, *13*, 8095.
[54] S. Q. Ali, A. Zehra, B. S. Naqvi, S. Shah, R. Bushra, *Oman Med. J.* **2010**, *25*, 294.
[55] B. F. Hettich, J. J. Bader, J.-C. Leroux, *Adv. Healthcare Mater.* **2022**, *11*, 2100047.
[56] G. Fuhrmann, A. Serio, M. Mazo, R. Nair, M. M. Stevens, *J. Controlled Release* **2015**, *205*, 35.
[57] L. Pascucci, V. Coccè, A. Bonomi, D. Ami, P. Ceccarelli, E. Ciusani, L. Viganò, A. Locatelli, F. Sisto, S. M. Doglia, E. Parati, M. E. Bernardo, M. Muraca, G. Alessandri, G. Bondiolotti, A. Pessina, *J. Controlled Release* **2014**, *192*, 262.
[58] G. Carobolante, J. Mantaj, E. Ferrari, D. Vllasaliu, *Pharmaceutics* **2020**, *12*, 226.
[59] D. Sun, X. Zhuang, X. Xiang, Y. Liu, S. Zhang, C. Liu, S. Barnes, W. Grizzle, D. Miller, H.-G. Zhang, *Mol. Ther.* **2010**, *18*, 1606.
[60] S. A. A. Kooijmans, S. Stremersch, K. Braeckmans, S. C. de Smedt, A. Hendrix, M. J. A. Wood, R. M. Schiffelers, K. Raemdonck, P. Vader, *J. Controlled Release* **2013**, *172*, 229.
[61] M. A. C. Pomatto, B. Bussolati, S. D'Antico, S. Ghiotto, C. Tetta, M. F. Brizzi, G. Camussi, *Mol. Ther. – Methods Clin. Dev.* **2019**, *13*, 133.
[62] K. L. Kotloff, M. S. Riddle, J. A. Platts-Mills, P. Pavlinac, A. K. M. Zaidi, *Lancet* **2018**, *391*, 801.
[63] M. Bardsley, C. Jenkins, H. D. Mitchell, A. F. W. Mikhail, K. S. Baker, K. Foster, G. Hughes, T. J. Dallman, *J. Clin. Microbiol.* **2020**, *58*, e01692.
[64] E. J. O'Donoghue, A. M. Krachler, *Cell. Microbiol.* **2016**, *18*, 1508.
[65] J. L. Kadurugamuwa, T. J. Beveridge, *J. Bacteriol.* **1996**, *178*, 2767.
[66] Z. Li, A. J. Clarke, T. J. Beveridge, *J. Bacteriol.* **1998**, *180*, 5478.
[67] J. Berleman, M. Auer, *Environ. Microbiol.* **2013**, *15*, 347.
[68] Z. Wang, Y. Ma, H. Khalil, R. Wang, T. Lu, W. Zhao, Y. Zhang, J. Chen, T. Chen, *Int. J. Nanomed.* **2016**, *11*, 4025.
[69] R. Shen, Y. Yu, R. Lan, R. Yu, Z. Yuan, Z. Xia, *Environ. Pollut.* **2019**, *254*, 112861.
[70] Y. Zhang, X. Wang, X. Yin, M. Shi, R. A. Dahlgren, H. Wang, *Environ. Toxicol.* **2016**, *31*, 736.
[71] S. Mostowy, L. Boucontet, M. J. Mazon Moya, A. Sirianni, P. Boudinot, M. Hollinshead, P. Cossart, P. Herbomel, J.-P. Levraud, E. Colucci-Guyon, *PLoS Pathog.* **2013**, *9*, e1003588.
[72] C. T. Chang, K. M. Doerr, C. M. Whipps, *J. Fish Dis.* **2017**, *40*, 1473.
[73] E. N. Faikoh, Y.-H. Hong, S.-Y. Hu, *Fish Shellfish Immunol.* **2014**, *38*, 15.
[74] X. Zhang, J. Song, A. Klymov, Y. Zhang, L. de Boer, J. A. Jansen, J. J. van den Beucken, F. Yang, S. A. Zaat, S. C. Leeuwenburgh, *Int. J. Nanomed.* **2018**, *13*, 5377.
[75] J. L. Kadurugamuwa, T. J. Beveridge, *Antimicrob. Agents Chemother.* **1998**, *42*, 1476.
[76] W. Huang, Q. Zhang, W. Li, M. Yuan, J. Zhou, L. Hua, Y. Chen, C. Ye, Y. Ma, *J. Controlled Release* **2020**, *317*, 1.
[77] R. Linnenberger, J. Hoppstädter, S. Wrublewsky, E. Ampofo, A. K. Kiemer, *Int. J. Mol. Sci.* **2021**, *22*, 12480.
[78] I. Wiegand, K. Hilpert, R. E. W. Hancock, *Nat. Protoc.* **2008**, *3*, 163.
[79] L. H. J. Richter, J. Herrmann, A. Andreas, Y. M. Park, L. Wagmann, V. Flockerzi, R. Müller, M. R. Meyer, *Toxicol. Lett.* **2019**, *305*, 73.